Mon. Not. R. Astron. Soc. **346,** 483–488 (2003)

Optical monitoring of the quasar 4C 38.41

B. Peng,★ J. Wu and X. Zhou

National Astronomical Observatories, Chinese Academy of Sciences, Datun Rd. A20, Chaoyang District, Beijing 100012, China

Accepted 2003 August 8. Received 2003 August 8; in original form 2003 June 10

ABSTRACT

The results of a photometric monitoring of the quasar 4C 38.41, performed at the optical *R* and *B* bands in 2002 February–March, are presented. With a 60/90 cm Schmidt telescope at the Xinglong station of the National Astronomical Observatories of China, we observed the source exhibiting amplitude variations of up to 0.78 mag in both bands during the whole campaign. Intraday and even intranight variations are detected as well. A typical variability time-scale of about 36 d is derived from our 2-month observations at the optical bands, which is identical to that found at a radio wavelength of 92 cm, suggesting a common origin for the variations in 4C 38.41 from optical to radio bands.

Key words: radiation mechanisms: non-thermal – methods: data analysis – galaxies: active – galaxies: photometry – quasars: individual: 4C 38.41.

1 INTRODUCTION

Many extragalactic radio sources have been found to show significant variability on time-scales of a few years, months or even periods as short as a day. The short time-scales of the variability, if intrinsic to the source, can give insights into the physics of the central energy source of the active nuclei.

The quasar 4C 38.41, at redshift $z = 1.814$, shows variability at high and low radio frequencies (e.g. Aller et al. 1985 and Peng & de Bruyn 1995). It has been classified as an optically violent variable (OVV) active galactic nucleus (AGN) (Mattox et al. 1993) because of its strong optical variability. Barbieri et al. (1977) reported the source light curve in the *B* band for 7 yr from 1969 May; the variations are visible on both long and short time-scales. The maximum brightness and the steepest big variations were observed by Villata et al. (1997) in the *R* band, where an outburst was detected with a brightness increase of 1.95 mag in 7 d after a period of quiet emission. The subsequent dimming phase was extremely rapid: an initial decrease of 1.08 mag was registered in 21 h, followed by another 1.11 mag in 3 d, after which the brightness returned to its 'normal' levels. Between these two drops, a noticeable intranight variability was detected when an increase $\Delta R = 0.34$ was registered in 35 min.

The quasar 4C 38.41 is one of the most powerful sources detected by the Energetic Gamma Ray Experiment Telescope (EGRET) (instrument on the Compton Gamma Ray Observatory). The γ-ray luminosity is at least two orders of magnitude larger than the maximum ever observed in any other band (Mattox et al. 1993). During 1992 November 17–December 1, 4C 38.41 was detected in the γ-ray band (>100 MeV); its flux varied by a factor of 1.5 within 24 h. It has been established for 4C 38.41 that enhanced levels of activity in the optical and γ-ray bands are associated with the emergence of new jet components (Barthel et al. 1995).

In this paper, we present new optical observations for the quasar 4C 38.41 over 2 months, between 2002 February and March (with an additional measurement on April 9 only in the *B* band), monitored by the 60/90 cm Schmidt telescope at the Xinlong station of the National Astronomical Observatories of the Chinese Academy of Sciences (NAOC), with aims to search for rapid variability at optical *R* and *B* bands simultaneously and possibly for typical time-scales. In the following section, observation and data reduction are described. We present the light curves and variability analysis in Section 3; discussion and conclusions are given in Section 4.

2 OBSERVATION AND DATA REDUCTION

An optical photometric monitoring on a program source 4C 38.41 was performed with the 60/90 cm Schmidt telescope at the Xinglong station of the NAOC, which is equipped with a Ford Aerospace 2048×2048 pixel^2 CCD camera with a 15-micron pixel size. The field of view of the CCD is 58×58 arcmin^2 with a plate scale of 1.7 arcsec pixel^{-1}. This telescope is mounted with 15 intermediate band filters covering a wavelength range from 300 to 1000 nm (e.g. Fan et al. 1996), over which filter i (666 nm) is the most sensitive one (Zhou et al. 2003).

2.1 Observation

The quasar 4C 38.41 is located at R.A. $16^{\rm h}35^{\rm m}15\overset{\rm s}{.}5$, Dec. $38^\circ08'04''$ (J2000) in the sky, which was monitored with two filters i (666 nm) and d (454 nm) of the 60/90 cm Schmidt telescope every night in the period of 2002 February to March, whenever the weather permitted. A total of 24 measurements in the i band and 28 in the d band were made. These filters are close to the *R* and *B* filters, respectively, in

★E-mail: pb@bao.ac.cn

© 2003 RAS

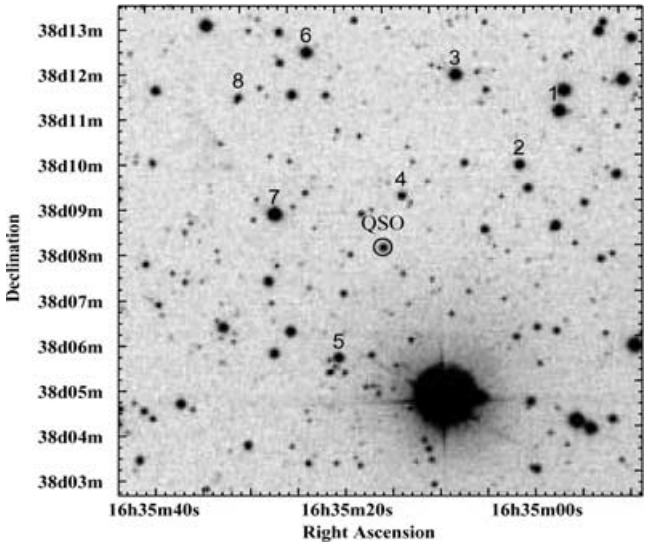

Figure 1. Image of the field of quasar 4C 38.41 observed with the 60/90 cm Schmidt telescope in the *R* band, where the 4C 38.41 and references stars are labelled by QSO, 1, 2, 3, . . . , 8 respectively.

the *UBVRI* system; hereafter, we refer to i and d bands as *R* and *B*, respectively. A typical exposure time lasted 20 min for the field centred on the program source 4C 38.41. In Fig. 1, we show an image of the field of quasar 4C 38.41 observed with the 60/90 cm Schmidt telescope in the *R* band, where the program source 4C 38.41 is denoted as QSO, and other reference stars are denoted as 1, 2, 3, 4, 5, 6, 7 and 8. These are located around 4C 38.41 and have brightness magnitudes close to it. The two reference stars 1 (R.A. $16^{\rm h}34^{\rm m}56\overset{\rm s}{.}59$, Dec. $38^\circ11'01\overset{''}{.}5$, J2000) and 6 (R.A. $16^{\rm h}35^{\rm m}23\overset{\rm s}{.}09$, Dec. $38^\circ12'26\overset{''}{.}6$, J2000) are taken arbitrarily to monitor the telescope stability.

The observational parameters are summarized in Tables 1 and 2 for *R* and *B* bands, respectively, with the observing epoch given in column 1 and the corresponding Julian Date (JD) given in column 2. On several occasions, the source was observed more than once in a photometric night to search for intranight variability.

2.2 Data reduction

The data reduction of the photometric observations was carried out with a 'Pipeline II' program based on the standard procedure of DAOPHOT (Stetson 1987), which has been developed to measure magnitudes of point sources in the BATC (Beijing–Arizona–Taipei–Connecticut) survey images (Zhou et al. 2003), consisting of four major steps: find all sources in the images; perform aperture photometry at 10 different radii of apertures; construct point spread function (PSF) fitting parameters and a look-up table with bright isolated stars; and perform PSF fitting to each point source and obtain its magnitude. In the automatic data reduction, most of the parameters in each step were fixed at their optimum values, leaving only a few – such as the FWHM of the object – to vary according to the seeing conditions at the time the image was taken. In a 1° field, the FWHM of the PSF can change by 0.2 arcsec from one place to another. This is because of the fact that the Schmidt focal plane is curved, whereas the CCD surface is flat (e.g. Fan et al. 1996).

The photometric system of this telescope defines the magnitude zero-points in a way similar to the spectrophotometric AB magnitude system introduced by Oke & Gunn (1983). The extinction

Table 1. Log of the optical observations and relative magnitudes for 4C 38.41 observed at the *R* band with the 60/90 cm Schmidt telescope of NAOC.

Observing epoch yyyy mm dd	Julian Date d	$m_r \pm \sigma_r$ mag
2002 02 04	245 2310.026	0.000 ± 0.018
2002 02 05	245 2311.063	0.010 ± 0.018
2002 02 08	245 2314.038	-0.091 ± 0.015
2002 02 08	245 2314.054	-0.085 ± 0.015
2002 02 09	245 2315.061	-0.054 ± 0.013
2002 02 10	245 2316.070	-0.103 ± 0.013
2002 02 12	245 2318.032	-0.161 ± 0.014
2002 02 12	245 2318.067	-0.187 ± 0.013
2002 02 13	245 2319.065	-0.175 ± 0.013
2002 02 14	245 2320.070	-0.138 ± 0.026
2002 02 15	245 2321.025	-0.291 ± 0.023
2002 02 15	245 2321.059	-0.231 ± 0.025
2002 02 16	245 2322.043	-0.187 ± 0.010
2002 02 16	245 2322.059	-0.201 ± 0.010
2002 02 17	245 2322.935	-0.167 ± 0.011
2002 02 18	245 2324.026	-0.207 ± 0.011
2002 02 21	245 2327.068	-0.167 ± 0.016
2002 02 26	245 2332.053	-0.238 ± 0.047
2002 03 02	245 2336.028	-0.248 ± 0.032
2002 03 05	245 2339.023	-0.045 ± 0.017
2002 03 07	245 2341.013	0.037 ± 0.027
2002 03 09	245 2343.022	-0.115 ± 0.016
2002 03 14	245 2348.028	0.138 ± 0.023
2002 03 28	245 2361.986	0.492 ± 0.100

Table 2. Log of the optical observations and relative magnitudes for 4C 38.41 observed at the *B* band with the 60/90 cm Schmidt telescope of NAOC.

Observing epoch yyyy mm dd	Julian Date d	$m_r \pm \sigma_r$ mag
2002 02 05	245 2311.079	0.000 ± 0.042
2002 02 06	245 2312.048	-0.056 ± 0.037
2002 02 06	245 2312.064	-0.011 ± 0.037
2002 02 08	245 2314.014	-0.087 ± 0.036
2002 02 09	245 2315.044	-0.053 ± 0.027
2002 02 10	245 2316.050	-0.106 ± 0.023
2002 02 12	245 2318.013	-0.138 ± 0.033
2002 02 13	245 2319.047	-0.150 ± 0.026
2002 02 14	245 2320.053	-0.111 ± 0.068
2002 02 15	245 2321.006	-0.115 ± 0.087
2002 02 15	245 2321.040	-0.104 ± 0.108
2002 02 16	245 2322.024	-0.143 ± 0.023
2002 02 17	245 2322.955	-0.070 ± 0.030
2002 02 18	245 2324.007	-0.144 ± 0.025
2002 02 21	245 2327.049	-0.033 ± 0.030
2002 02 26	245 2332.037	-0.094 ± 0.123
2002 02 27	245 2332.986	-0.312 ± 0.148
2002 02 27	245 2333.019	-0.071 ± 0.156
2002 03 02	245 2336.010	-0.208 ± 0.093
2002 03 05	245 2339.008	-0.005 ± 0.046
2002 03 07	245 2341.001	-0.021 ± 0.039
2002 03 09	245 2343.010	-0.066 ± 0.026
2002 03 14	245 2348.041	0.117 ± 0.033
2002 03 23	245 2357.020	0.145 ± 0.075
2002 03 23	245 2357.029	0.173 ± 0.082
2002 03 28	245 2361.996	-0.013 ± 0.198
2002 03 28	245 2362.007	-0.266 ± 0.154
2002 04 09	245 2373.979	0.430 ± 0.054

coefficients at any given time in a night and the zero-point of the instrumental magnitude are derived from the images of standard stars. The error in magnitude for a single star is obtained from the comparison of the magnitudes in a short exposure with that from the combined image. The total measuring error comes from bias (over-scan) correction and CCD readout noise, flat-field correction, photometry of PSF fitting and calibration error. According to Zhou et al. (2003), the main error in magnitude is the photometric error of PSF fitting due to the statistical photon-counting error and the sky background noise, depending on the brightness of the objects.

The results of the optical observations are summarized in the last column in Tables 1 and 2 for *R* and *B* bands, respectively, where the magnitudes relative to the first epoch are listed, and the corresponding uncertainties are estimated by combining in quadrature the uncertainties of the target source with that of the zero-point of the calibration stars.

3 RESULTS

3.1 Light curves of 4C 38.41

The light curves of the quasar 4C 38.41 and selected reference stars at the *R* ($\lambda 666 \pm 24$nm) band are demonstrated in Fig. 2, where the top panel shows the magnitudes of 4C 38.41 (m_i) relative to that of its first epoch (m_1), i.e. $m_r = m_i - m_1$; the bottom panel shows the magnitude difference between the two reference stars ($m_6 - m_1$). The horizontal axis is the observing epoch in days of JD 245 2300. Similarly, the light curves of 4C 38.41 and the same two reference stars at *B* ($\lambda 454 \pm 17$nm) band are displayed in Fig. 3. The error in the *B* band is obviously larger than that in the *R* band, which is due to the brightness difference of the same stars and the sensitivity of the CCD at different wavelengths.

From the light curves, we observed that the general trends at both *R* and *B* bands are the same, i.e. the source 4C 38.41 exhibited amplitude oscillations with similar increase and decrease there. This can be quantified in Table 3, where the I or D refers to a flux increase or decrease, respectively, in each defined time interval. Because the scatter in the *B* band is found to be larger than that in the *R* band, we will only analyse variability behaviour of the quasar 4C 38.41 in the *R* band. It is evident that, in the *R* band, the most pronounced variations were measured first with a decrease of 0.29 mag in 5 d between JD 245 2336 and 245 2341, followed by an increase of 0.15 mag in 2 d and then a decrease of 0.25 mag in 5 d. A further decay of 0.35 mag lasted until the end of the observation, but was recorded by only one measurement with larger uncertainty. We can summarize that the maximum change was 0.78 mag in the *R* band over the period of JD 245 2310 and 245 2362, during which it was 0.49 mag in the *B* band. It will be of 0.74 mag in the *B* band when an additional observation in 12 d after the end of the *R* one is included.

Another important observational finding, which can be identified from the light curves, is intraday variability at some epochs, notably between JD 245 2315 and 245 2316 (a detection over 3σ) and between JD 245 2320 and 245 2321 at the *R* band (over 3σ); even intranight variability was identified with three measures in the night of JD 245 2322 (over 3σ). Therefore, both intraday and intranight amplitude changes are detected in 4C 38.41.

3.2 Statistical analysis

The rms of (the magnitude difference of) the two reference stars are estimated to be 0.010 mag at the *R* band and 0.025 mag at the *B* band, respectively; this indicates the telescope stability and the mean error of our photometric measurements. This also demonstrates that the *R*-band photometry is more sensitive than the *B*-band photometry.

To see whether a source is variable, we performed a χ^2 test: $\chi^2 = \sum[(m_r - \langle m_r \rangle)/\sigma_r]^2$ (following, for example, Fanti et al. 1981), where the m_r are the individual relative magnitudes, the σ_r

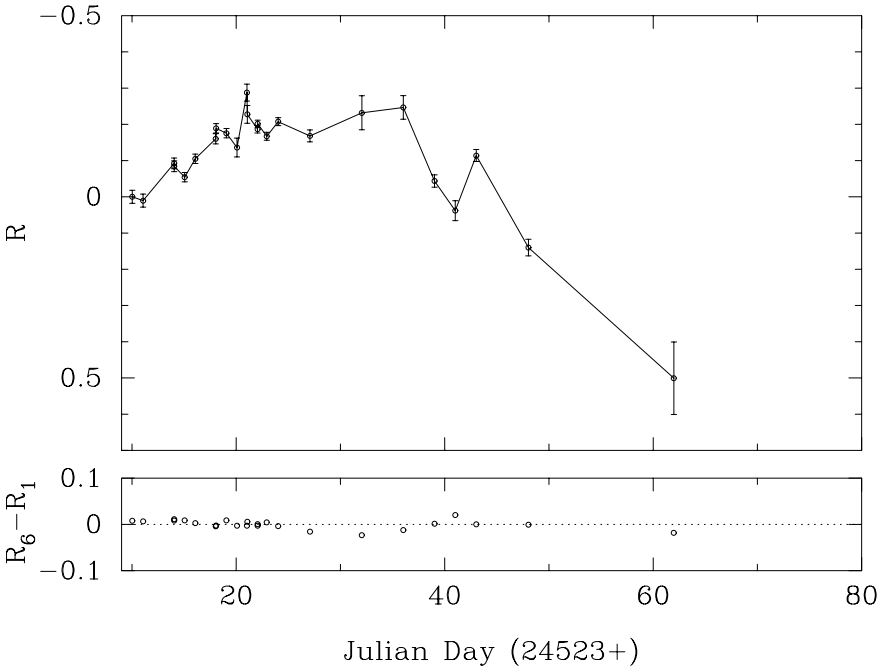

Figure 2. Light curves of the quasar 4C 38.41 and two selected reference stars 1 and 6 at the *R* band, observed with the 60/90 cm Schmidt telescope of the NAOC.

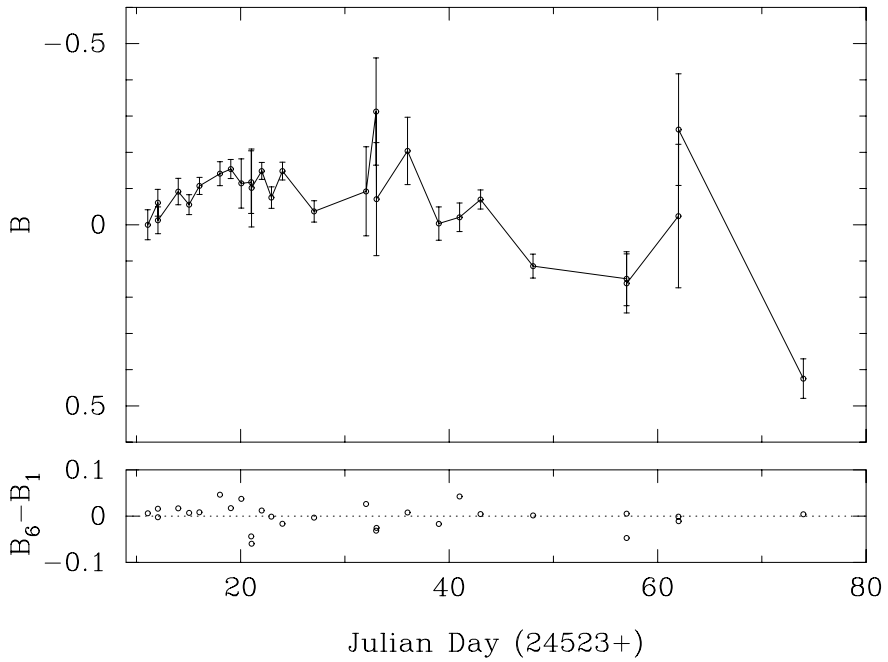

Figure 3. Light curves of the quasar 4C 38.41 and two selected reference stars 1 and 6 at the *B* band, observed with the 60/90 cm Schmidt telescope of the NAOC.

Table 3. Maximum amplitude changes in different time intervals at the *R* and the *B* bands, where I or D refers to the increase or decrease in flux.

Time interval (d) JD 245 23XX	Maximum change (mag) R	B	Notes I or D
10–21	0.30	0.15	I
21–36	0.08	0.28	I
36–41	0.29	0.20	D
41–43	0.15	0.05	I
43–48	0.25	0.18	D
48–62	0.35	0.06	D

are the corresponding uncertainties listed in Tables 1 and 2, and $\langle m_r \rangle$ denotes the mean (relative) magnitude at each band. The reduced $\chi^2_{\rm red}$ values are calculated to be 35.2 for the data set of the *R* band and 7.1 for that of the *B* band, respectively, confirming statistically that the quasar 4C 38.41 is variable at a confidence level of more than 99.95 per cent at both wavelengths, namely 666 and 454 nm.

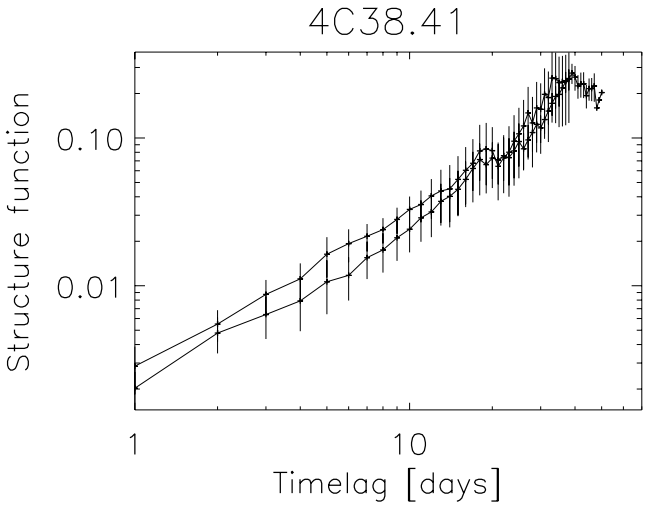

Figure 4. Structure function of the quasar 4C 38.41 at *R* band.

3.3 Variability time-scale

Structure functions (Simonetti, Cordes & Heeschen 1985) can be used to search for typical time-scales and periodicities. A characteristic time-scale in a light curve, defined as the time interval between a maximum and an adjacent minimum or vice versa, is indicated by a maximum of the structure function, whereas a periodicity in the light curve causes a minimum of the structure function (Heidt & Wagner 1996). Each structure function was derived twice by using an interpolation algorithm, first starting from the beginning of the time series, and secondly starting at the end and proceeding backwards. This provides a rough assessment of the errors caused by the interpolation process.

In Fig. 4, we plot the structure function $D(\tau) = \langle [m_r(t) - m_r(t + \tau)]^2 \rangle_t$ of the amplitude for all epochs at the *R* band, where $\langle\ \rangle_t$ is the mean over time. The structure function shows a clear maximum at $\tau \sim 36 \pm 3$ d, but no typical periodic time-scales can be identified. The maximum in the structure function we obtained is on time-scales longer than half the monitoring period, and is therefore less well defined according to the sampling theorem. In the absence of a proper statistical test of the irregular sampling one normally has, one can argue that the error bars will roughly increase linearly with period if only independent pairs of data are used to measure the variability. In our case, the time-scale of 36 d is thus suggestive only.

We then conclude that 4C 38.41 is variable at both the *R* and the *B* bands on a typical time-scale of ∼36 d, although the *B* band has larger scatter.

4 DISCUSSION AND CONCLUSION

Variability has been used to probe the physical processes of AGNs. When explaining new observational results, the shocks-in-jet model seems to be more reasonable than other models (Wagner & Witzel 1995).

4.1 Shocks-in-jet model

The relativistic beaming hypothesis and the unified scheme for AGNs (Schlickeiser 1996) are supported by the observation of non-thermal γ-ray radiation from flaring blazars.

For 4C 38.41, strong γ-ray variability was found during 1991 April and 1995 September in the first 4.5 yr of EGRET operation (Mukherjee et al. 1997). Some simultaneous observations with *ASCA* and EGRET reported time variability for 4C 38.41 (Kubo et al. 1998). The γ-ray flare is often accompanied by a flare at low frequencies (Reich et al. 1993). On the other hand, the short time-scale variability of a few months at centimetre wavelengths found for 4C 38.41 implies such a high brightness temperature that bulk relativistic motions of the synchrotron-emitting plasma at viewing angles close to the line of sight have to be invoked – for example, rapid variability on a time-scale of a month at 327 MHz detected by Peng & de Bruyn (1995), and evidence of superluminal motion in 4C 38.41 provided by Barthel et al. (1995).

Because the physical quantities in the jet are assumed to change in a continuous way with distance, the corresponding light curve should change in a continuous way without any plateau. This seems consistent with what we observed, i.e. the source flux varied up and down smoothly at both the *R* and the *B* bands. Flares in the optical should lag analogous flares in the ultraviolet, and lead flares in the infrared, as the shock propagates from the inner to the outer jet. Unfortunately, we lack data in other wavebands during our monitoring period; therefore, we are not able to verify this model.

4.2 VLBI structure

Very Large Baseline Interferometry (VLBI) observations at 5 GHz (Pearson & Readhead 1988) show a structure in 4C 38.41 with three components. At 608 MHz (Padrielli et al. 1991), there is a compact core with an extended structure to the west up to 20 mas and some indication of the extension to the east up to 10 mas. Global Mark 2 VLBI snapshot observations at 92 cm (Altschuler et al. 1995) reveal both some extension to the east ($<$20 mas) and greater extension to the northwest along a position angle of -35°. Such a structural pattern at the range of frequencies from 327 MHz to 5 GHz is typical for a core-jet morphology. The submilliarcsecond images (Kellermann et al. 1998) at 15 GHz by the Very Long Baseline Array (VLBA) classified the core-jet structure of 4C 38.41 as single-sided, which is the result of differential Doppler boosting of an intrinsic twin-jet structure. Doppler boosting enhances one side as the relativistic motion is observed at small viewing angle.

4.3 Conclusion

Our optical observations with the 60/90 cm Schmidt telescope revealed variations of the source 4C 38.41, on both long and short time-scales, with a maximum variation of 0.78 mag in the *R* band and 0.74 mag in the *B* band. We discussed *R* band variations mostly because they have higher accuracy. Nevertheless, it is noticed that the *R* band amplitudes are larger; this would be unusual for a pure synchrotron spectrum where variations are often larger at higher photon energies. It may point to a significant contribution of thermal emission, which is blue and variable only on longer time-scales. The thermal, steady contribution dilutes the synchrotron radiation in the *B* band and might be the reason for the lower amplitude here.

Trends on long time-scales of days to weeks are recognizable, while some fast variations over a day and even intra-night were detected. We further derived a time-scale of about 36 d, although not with high confidence, which is similar to the previously measured time-scale of 35 d at 92 cm (Peng 2002), suggesting a common origin for the variability from optical to radio bands.

In light of the variations over the broad wavebands from radio to γ-ray, the cause is likely to be intrinsic to the source. The dynamic process may lead to variations of the projected size of the source or the viewing angles of the line of sight with respect to the direction of emission. Jets in quasars may be powered by rotating black holes in the nuclei (Blandford & Znajek 1977; Moderski, Sikora & Lasota 1998). Our optical result supports the intrinsic mechanism discussed for the radio variations at 327 MHz, which could be caused either by a small change of the viewing angle or by a small diameter variation as discussed in Peng & de Bruyn (1995).

ACKNOWLEDGMENTS

The authors thank the 60/90 cm Schmidt telescope team for helping the observations. We are grateful to Stefan Wagner for his careful reading of the paper and for sending us valuable comments. We used the computing programme of the IDV group at MPIfR in Germany when deriving the structure function. This research has made use of NASA's Astrophysics Data System Abstract Service and of the NASA/IPAC Extragalactic Data base (NED) which is operated by the Jet Propulsion Laboratory, Caltech, under contract with the National Aeronautics and Space Administration. This research is supported by the National Nature Science Foundation of China through grant no. 10173015.

REFERENCES

Aller H. D., Aller M. F., Latimer G. E., Hodge P. E., 1985, ApJS, 59, 513
Altschuler D. R., Gurvits L. I., Alef W., Dennison B., Graham D., Trotter A. S., Carson J. E., 1995, A&AS, 114, 197
Barbieri C., Romano G., di Serego S., Zambon M., 1977, A&A, 59, 419
Barthel P. D., Conway J. E., Myers S. T., Pearson T. J., Readhead A. C. S., 1995, ApJ, 444, L21
Blandford R. D., Znajek R. L., 1977, MNRAS, 179, 433
Fan X. et al., 1996, AJ, 112, 628
Fanti C., Fanti R., Ficarra A., Mantovani F., Padrielli L., Weiler K. W., 1981, A&AS, 45, 61
Heidt J., Wagner S. J., 1996, A&A, 305, 42
Kellermann K. I., Vermeulen R. C., Zensus J. A., Cohen M. H., 1998, ApJ, 115, 1295
Kubo H., Takahashi T., Madejski G., Tashiro M., Makino F., Inoue S., Takahara F., 1998, ApJ, 504, 693
Mattox J. R. et al., 1993, ApJ, 410, 609
Moderski R., Sikora M., Lasota J. P., 1998, MNRAS, 301, 142
Mukherjee R. et al., 1997, ApJ, 490, 116
Oke J. B., Gunn J. E., 1983, ApJ, 266, 713
Padrielli L., Eastman W., Gregorini L., Mantovani F., Spangler S., 1991, A&A, 249, 351

Pearson T. J., Readhead A. C. S., 1988, ApJ, 328, 114
Peng B., 2002, MNRAS, 330, 344
Peng B., de Bruyn A. G., 1995, A&A, 301, 25
Reich W., Steppe H., Schlickeiser R., Reich P., Pohl M., Reuter H. P., Kanbach G., Schonfelder V., 1993, A&AS, 273, 65
Schlickeiser R., 1996, A&AS, 120, 481
Simonetti J. H., Cordes J. M., Heeschen D. S., 1985, ApJ, 296, 46
Stetson P. B., 1987, PASP, 99, 191
Villata M., Raiteri C. M., Ghisellini G., de Francesco G., 1997, A&AS, 121, 119
Wagner S. J., Witzel A., 1995, ARA&A, 33, 163
Zhou X. et al., 2003, A&A, 397, 361

This paper has been typeset from a TEX/LATEX file prepared by the author.